Available online at www.sciencedirect.com
SCIENCE DIRECT
Polymer 47 (2006) 3705–3710
polymer
www.elsevier.com/locate/polymer

Polymer Communication

Single wall carbon nanotube templated oriented crystallization of poly(vinyl alcohol)

Marilyn L. Minus, Han Gi Chae, Satish Kumar *

School of Polymer, Textile and Fiber Engineering, Georgia Institute of Technology, P.O. Box 0295, Atlanta, GA 30332-0295, USA

Received 5 November 2005; received in revised form 18 March 2006; accepted 22 March 2006

Abstract

Shearing of poly(vinyl alcohol) (PVA)/single wall carbon nanotube (SWNT) dispersions result in the formation of self-assembled oriented PVA/SWNT fibers or ribbons, while PVA solution results in the formation of unoriented fibers. Diameter/width and length of these self-assembled fibers was 5–45 μm and 0.5–3 mm, respectively. High-resolution transmission electron micrographs showed well resolved PVA (200) lattice with molecules oriented parallel to the nanotube axis. Nanotube orientation in the self-assembled fibers was also determined from Raman spectroscopy. PVA fibers exhibited about 48% crystallinity, while crystallinity in PVA/SWNT fibers was 84% as determined by wide angle X-ray diffraction. PVA and carbon nanotubes were at an angle of 25–40° to the self-assembled fiber axis. In comparison to PVA, PVA/SWNT samples exhibited significantly enhanced electron beam radiation resistance. This study shows that single wall carbon nanotubes not only nucleate polymer crystallization, but also act as a template for polymer orientation.

Keywords: Poly(vinyl alcohol); Carbon nanotubes; Orientation

1. Introduction

Self-assembly and crystallization of polymers from stirred/sheared polymer solutions was first reported in 1960s [1–7]. The observation of the shish-kebab structure with extended core in polyethylene from such crystals may be credited for the ultimate development, and commercialization of extended chain polyethylene fiber in 1980s [8]—an important milestone in the processing of high performance fibers from flexible polymers. After over 60 years of development in fiber processing technology, the basic morphological structure of commodity polymeric fibers such as nylon 6, nylon 66, polypropylene, and poly(ethylene terephthalate) (PET), has not changed significantly over the years. A number of recent studies demonstrate that single wall carbon nanotubes act as a nucleating agent for polymer crystallization [9–17]. Oriented crystallization of small molecules such as sulfuric acid can also occur on SWNT surface [18]. Poly(vinyl alcohol) (PVA) has played a critical role in single wall carbon nanotube processing [10,19–23]. Macroscopic fibers from SWNTs were for the first time processed in PVA solutions [24]. Super tough fibers have also been processed from PVA/SWNT composites [25]. In this study, we report that stirred and sheared solutions of PVA result in the formation of isotropic fibers with low crystallinity, while under comparable conditions PVA/SWNT dispersions result in oriented fibers with high crystallinity.

2. Experimental

Atactic poly(vinyl alcohol) (PVA) (from Kuraray Co. Ltd, lot no. 636837, degree of polymerization: 18,000, and 98.4% hydrolyzed) was dissolved in an 80:20 volume ratio of dimethyl sulfoxide (DMSO) (from J.T Baker Cas. No. 67-68-5) and distilled water, respectively, in a 1 L three-necked round-bottomed flask equipped with a magnetic stir bar and Liebig condenser assembled for reflux and heated to 110 °C to obtain a 1 wt% PVA solution (80 ml DMSO, 20 ml water, and 1.1 g PVA). SWNT (obtained from CNI, lot no. P0247, purity >98%) (10 mg/ml) dispersion was obtained in DMSO by sonicating (using a Fisher FS30 bath sonicator, frequency 43 kHz, power 150 W) for 12 h at 55 °C and subsequently added to the PVA solution to obtain PVA:SWNT weight ratio of 99:1. The mixture was stirred with an overhead mechanical stirrer (Caframo high shear mixer, model no. BDC1850) at shear speeds between 500 and 800 rpm continuously for 72 h. Dispersion was periodically sonicated

* Corresponding author. Tel.: +1 404 894 7550; fax: +1 404 894 8780.
E-mail address: satish.kumar@ptfe.gatech.edu (S. Kumar).

0032-3861/$ - see front matter © 2006 Elsevier Ltd. All rights reserved.
doi:10.1016/j.polymer.2006.03.076

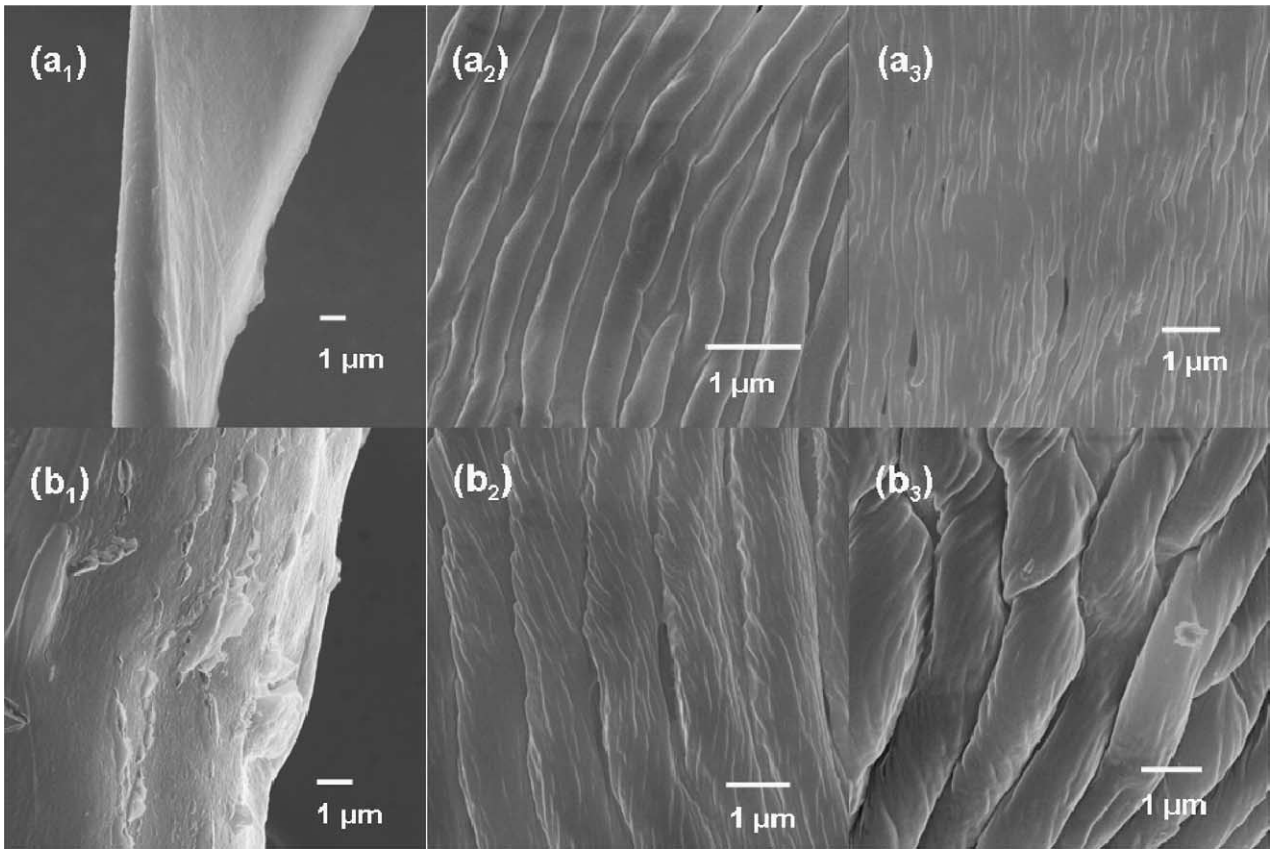

Fig. 1. Scanning electron micrographs of self-assembled (a) PVA and (b) PVA/SWNT fibers. (a_1) and (b_1) fiber surface, (a_2, a_3) and (b_2, b_3) internal surface obtained by fiber splitting.

for about 10 min after every 2 h while stirring. The same procedure was carried out for PVA solution without nanotubes. Macroscopic fibers formed in each solution within 2 h of stirring, and no change was observed after about 6 h. Continuous sonication results in dissolution of these fibers. Fibers were placed on a glass slide and dried in the hood for several days followed by drying under vacuum at 30 °C for 72–96 h.

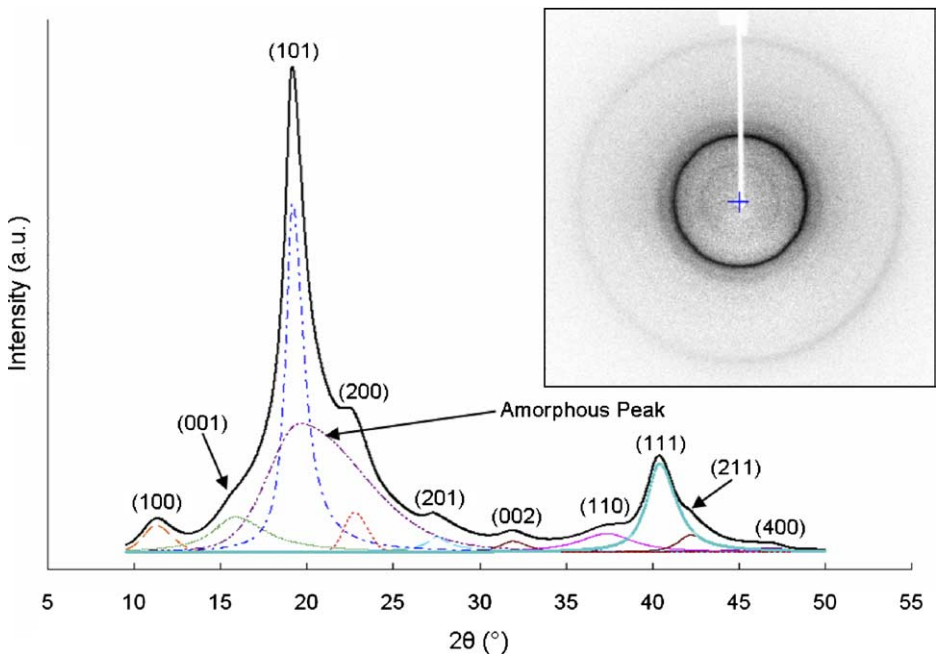

Fig. 2. Peak fitted integrated X-ray diffraction intensity as a function of 2θ of self-assembled PVA fiber. Inset-wide angle X-ray diffraction pattern with vertical fiber axis.

Scanning electron microscopy was done on LEO 1530 thermally assisted field emission microscope (at 10 kV) on samples sputtered coated with gold. To reveal the internal fiber structure, both PVA and PVA/SWNT fibers were split using a needle for SEM observation. Transmission electron microscopy (TEM) was done on Hitachi HD-2000 Field Emission Gun electron microscope (accelerating voltage 200 kV). TEM samples were prepared by taking a drop of fibril containing dispersion using a pipette and dropping it on lacey carbon coated 300 mesh copper grids (Electron Microscopy Sciences Cat. no. 71140). This grid was dried under hood for several days. Raman spectroscopy was done on a Holoprobe Raman microscope by Kaiser Optical Systems Inc., at an excitation wavelength of 785 nm and 1.5 MW beam power. Leica DMRX Optical Microscope manufactured by Leica Microsystems equipped with a Sony Digital Photo Camera DKC-5000 was used to image the fibers and study their birefringent behavior. Wide angle X-ray scattering was done on the Rigaku Micro Max 002 X-ray generator operated at 45 kV and 0.66 mA and equipped with *R*-axis VI++ detector. For X-ray studies, single filaments were mounted on the tip of a 0.3 mm diameter glass fibers (Hamilton Research Cat. no. HR8-030). Crystallinity and orientation from wide angle X-ray diffraction were determined using the software MDI Jade 6.1. AreaMax software was used for background subtraction and integration. The area due to the crystalline and amorphous contribution of the polymer was determined by peak fitting analysis.

3. Results and discussion

Diameter/width of both the PVA and PVA/SWNT self-assembled fibers/ribbons is in the range of 5–45 μm, and the length is typically from 0.5 to 3 mm. Both the PVA and PVA/SWNT fibers are composed of fibrils ranging from about 100 to 800 nm in diameter (Fig. 1). The PVA/SWNT fibrils also appear to consist of nano fibrils ranging from 25 to about 100 nm in diameter, while the PVA fibrils did not show the obvious presence of nano fibrils. Wide-angle X-ray scattering and polarizing optical microscopy, both show that PVA fibers are isotropic (Fig. 2) while PVA/SWNT fibers are oriented (Figs. 3 and 4). For brevity optical micrograph of the isotropic PVA fiber is not included.

Wide angle X-ray diffraction (WAXD) of the self-assembled PVA fibers show strong intensity (101) peak (Fig. 2), which is also the case for solution spun and drawn PVA fibers [26,27]. In the self-assembled PVA/SWNT fibers, medium intensity (101) reflection is observed as a four-point pattern at 32.2° off the meridian. Strong intensity (200) reflection is present on the equator, and the (102) plane is on the meridian (Fig. 3(b)). Various crystal sizes determined from WAXD data using Scherrer equation [28] (using $K=0.9$) as well as *d*-spacing values in both PVA and PVA/SWNT fibers are listed in Table 1. The crystallinity in self-assembled PVA and PVA/SWNT fibers, determined using crystalline and amorphous peak areas, was about 48 and 84%, respectively, (Figs. 2 and 3). It is noted that crystallinity in gel spun

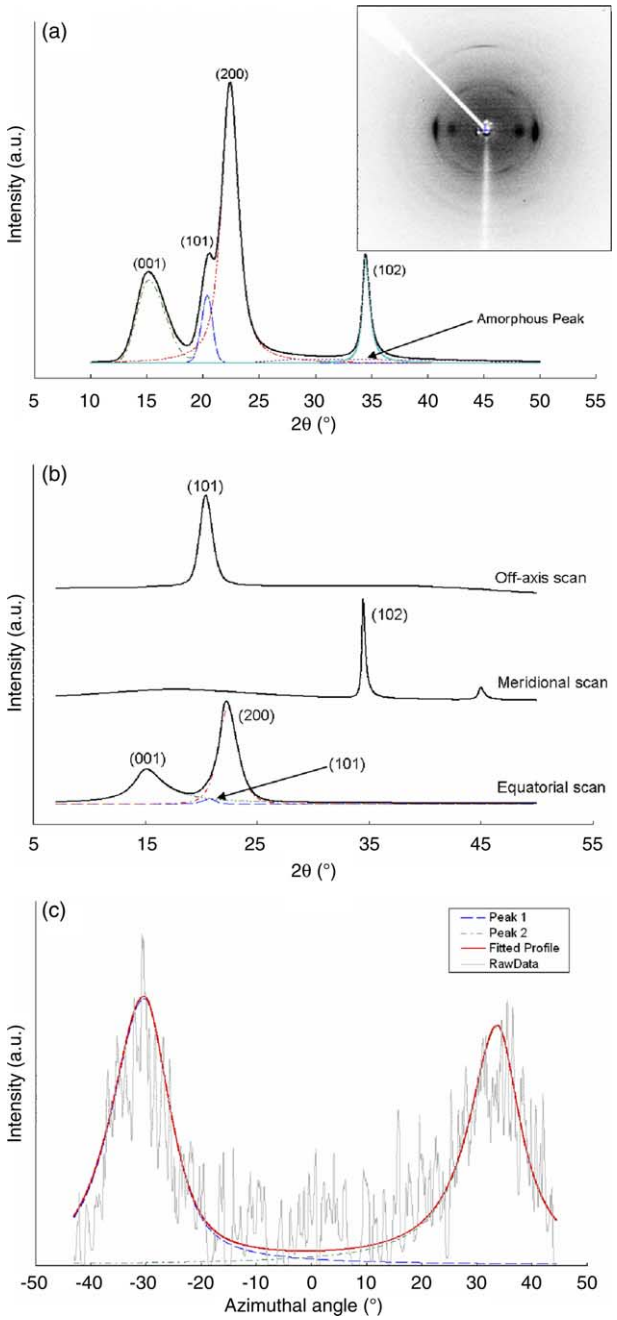

Fig. 3. Wide angle X-ray diffraction of self-assembled PVA/SWNT fiber. (a) Peak fitted integrated intensity as a function of 2θ. Inset-WAXD pattern with vertical fiber axis. (b) Equatorial, meridional, and off-axis (from 32.2° from the meridian) intensity as a function of 2θ. (c) Azimuthal intensity plot for the (101) diffraction plane. 0° represents the meridional direction.

PVA/SWNT fiber (draw ratio 6), containing 3 wt% SWNT was only ~53% [10]. It is also noteworthy that 84% crystallinity in the current work is without annealing or drawing.

PVA orientation factor, f_b, was determined from (200) and (001) diffraction planes using Wilchinsky's equation [29]:

$$\overline{\cos^2\theta_{b-\text{axis}}} = 1 - \frac{(1-2\sin^2\rho_2)(\overline{\cos^2\phi_1}) - (1-2\sin^2\rho_1)(\overline{\cos^2\phi_2})}{\sin^2\rho_1 - \sin^2\rho_2} \quad (1)$$

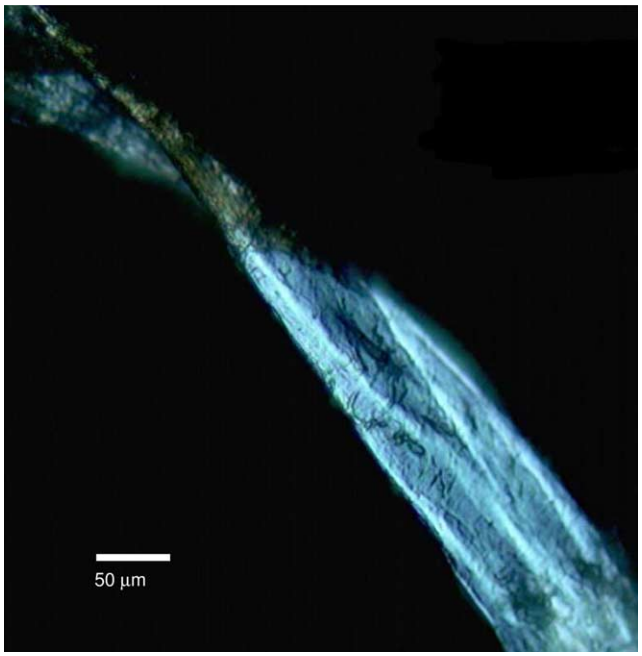

Fig. 4. Optical micrograph of self-assembled PVA/SWNT fiber under cross polarizers. Fiber axis is at 45° to the polarization direction.

The subscripts, 1 and 2 refer to the two planes, (200) and (001), used in the orientation characterization, and ρ is the angle between the given plane normal and the a- or c-axis. PVA unit cell parameters are [30]: $a=7.81$ Å, $b=2.52$ Å, $c=5.51$ Å, $\beta=91.7°$. Thus, ρ values for (200) and (001) are calculated with respect to the a-axis to be 0 and 88.3°, respectively. The (200) and (001) azimuthal intensity was used to calculate $\cos^2\phi_{h0l}$ for the two planes. Using this approach $\cos^2\theta_{b-\text{axis}}$, and f_b in the PVA/SWNT fiber was calculated to be 0.82, and 0.72, respectively, giving PVA misorientation angle of about 26° with respect to the fiber axis.

Fig. 3(c) shows the (101) intensity as a function of azimuthal angle. The angle between (101) plane normal and the self-assembled fiber axis (α) was calculated using the following equation [31]

$$\cos\delta = \frac{\cos\alpha}{\cos\theta} \tag{2}$$

where δ is the azimuthal angle between the diffraction maximum and the meridian direction as measured from the X-ray, and θ is the (101) Bragg angle. The values for δ and θ measured from WAXD were 32.2 and 10.2°. From these parameters, α was calculated to be 33.6°, while the theoretical value based on above listed unit cell parameters would be

Table 1
X-ray determination of d-spacing and crystal size for predominant planes in both self-assembled PVA and PVA/SWNT fiber diffraction patterns

Diffraction plane	Self-assembled PVA/SWNT fiber			Self-assembled PVA fiber		
	2θ (°)	d-spacing (nm)	Crystal size (nm)	2θ (°)	d-spacing (nm)	Crystal size (nm)
(100)	–	–	–	11.3	0.785	4.2
(001)	15.5	0.571	3.1	15.8	0.559	2.2
(101)	20.4	0.434	6.3	19.5	0.453	6.6
(200)	22.9	0.387	6.2	22.7	0.390	5.8
(102)	34.5	0.259	9.7	–	–	–
(111)	–	–	–	40.3	0.201	4.3

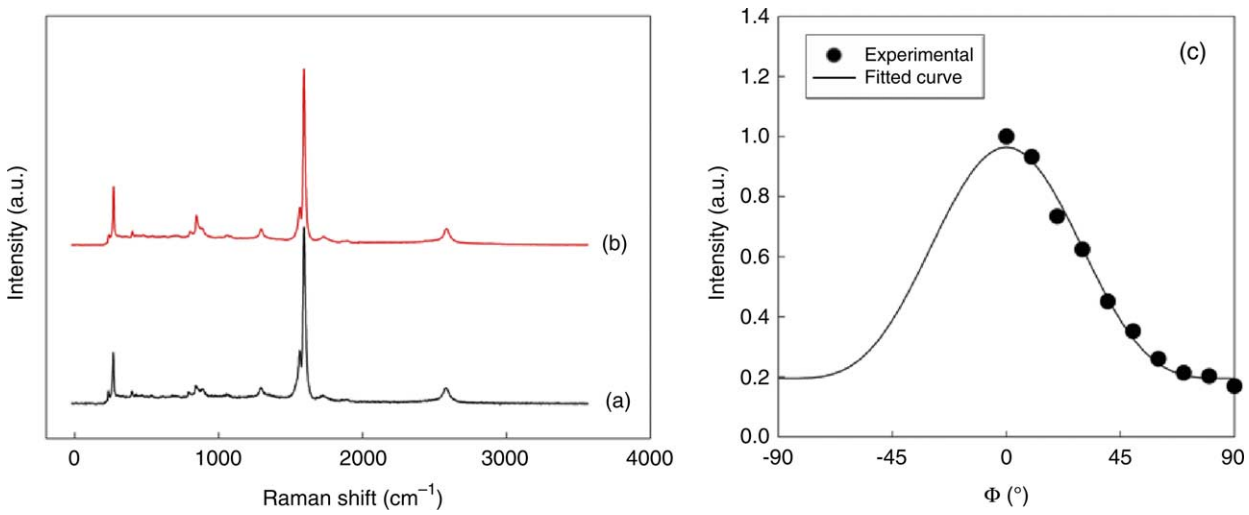

Fig. 5. Raman spectra of (a) SWNT powder and (b) self-assembled PVA/SWNT fiber. (c) Polarized tangential mode (G-band) Raman intensity for the self-assembled PVA/SWNT fibers as a function of angle between polarization direction and the fiber axis.

35.2°. Peak-fitting analysis of the equatorial WAXD scan of the self-assembled PVA/SWNT fiber also shows a low intensity (101) peak on the equator (Fig. 3(b)), suggesting two distinctly different orientations of the PVA molecules in the self-assembled fiber.

The presence of SWNTs in fibers assembled from PVA/SWNT dispersion was confirmed by Raman spectroscopy (Fig. 5(a)), where the Raman spectrum of the self-assembled fiber is compared to the spectrum of the SWNT powder. Due to resonance enhanced Raman scattering, SWNT intensity dominates and no PVA peaks were observed in the Raman spectra even at this low SWNT concentration. As can be seen in Fig. 5a and b, Raman spectrum of the PVA/SWNT fiber is nearly identical to the SWNT powder spectra. Polarized G-band Raman intensity as a function of the angle between the polarization direction and fiber axis is given in Fig. 5(c). The average SWNT orientation with respect to the fiber axis was calculated using a previously described method [32,33] from the polarized Raman G-band intensity as a function of polarization angle. SWNT orientation factor was determined to be 0.44, which yields an approximate SWNT orientation angle of about 38° from the self-assembled fiber axis.

High-resolution transmission electron micrograph in Fig. 6(a) shows a PVA/SWNT nano fibril of about 120 nm diameter. Higher magnification lattice images of this nano fibril (Fig. 6(b) and (c)) show well resolved (200) lattice planes as well as the presence of SWNT. (200) plane and hence the *b*-axis (the PVA chain axis) is parallel to the SWNT axis and both are in turn perpendicular to the nano fibril axis. Moire [34] patterns can also be seen in Fig. 6(b) (indicated by arrow). Fig. 6 shows significantly larger crystal sizes, both along and perpendicular to the *b*-axis direction, than the average crystal sizes observed from X-ray. It is also noted that PVA/SWNT fibrils were highly resistant to the electron beam. Under comparable electron beam irradiation conditions, PVA samples without nanotubes could not be lattice imaged. Similarly, polyacrylonitrile/SWNT composites were found to be more radiation resistant than polyacrylonitrile [33].

WAXD and Raman spectroscopy show PVA and SWNT orientation. However, the two orientation values were somewhat different. High-resolution transmission electron micrograph (Fig. 6), provided unequivocal evidence that PVA molecules are oriented parallel to the nanotube axis. In summary, we conclude that the presence of SWNTs, results in significantly enhanced polymer crystallinity, and that SWNTs act as a template for polymer orientation. While there are a number of previous studies in the literature reporting enhanced crystallinity [11,14,15] and crystallization [13,35] rate in polymers in the presence of carbon nanotubes and particularly single wall carbon nanotubes, here we show SWNT templated polymer orientation in solutions. SWNT templated polymer orientation has also been reported recently during melt processing [36]. Polymer orientation facilitated by the presence of fully exfoliated SWNTs may have implications for polymer processing.

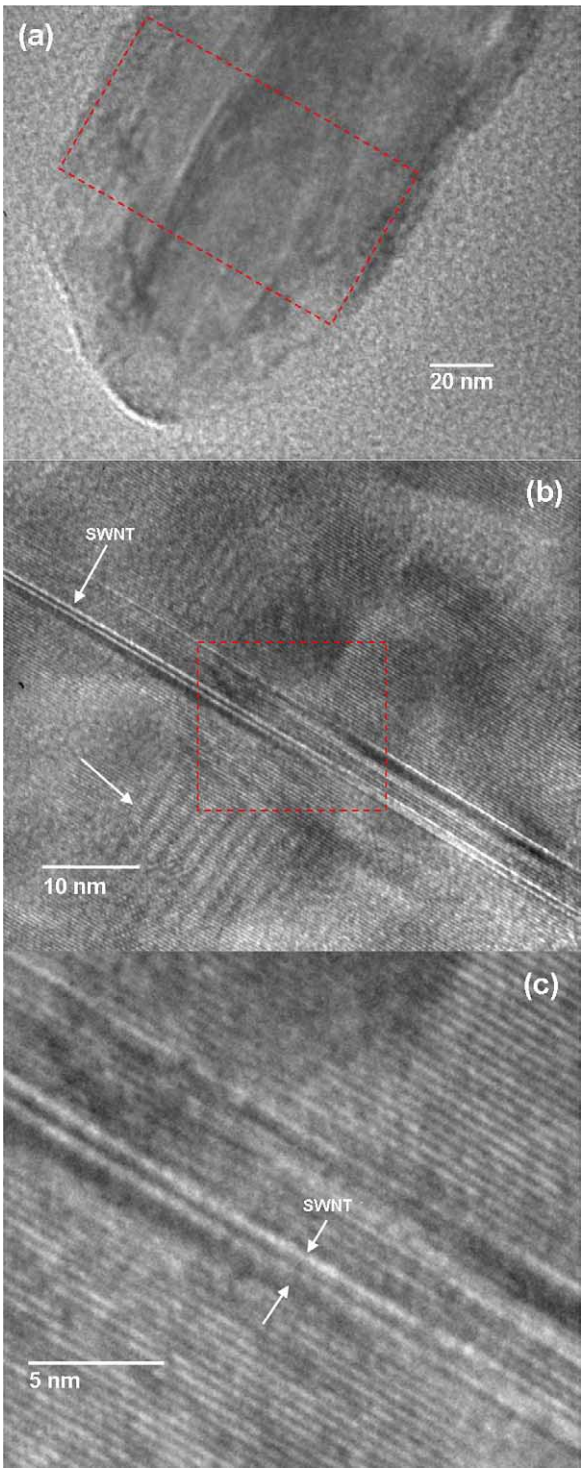

Fig. 6. Transmission electron micrographs of self-assembled PVA/SWNT nano fibril. (b) is a higher magnification image of the boxed region in (a). (c) is a higher magnification image of the boxed region in (b). Nano fibril diameter is about 120 nm. SWNT and PVA (200) lattice planes (*d*-spacing ~0.385 nm) parallel to SWNT axis can be clearly seen in (b) and (c).

Acknowledgements

This worked was funded by ONR (N00014-01-1-0657), AFOSR (F49620-03-l-0124), and Carbon Nanotechnologies, Inc.

References

[1] Pennings AJ, Kiel AM. Colloid Polym Sci 1965;205:160–2.
[2] Wikjord AG, Manley RS. Can J Chem 1969;47:703.
[3] Pennings AJ, van der Mark JMAA, Booji HC. Colloid Polym Sci 1970; 236:1435–536.
[4] Pennings AJ, Zwijnenb A, Lagereen R. Kolloid-Z Z Polym 1973;251:500–1.
[5] Matsuzaw S, Yanagisa H, Yamaura K. Colloid Polym Sci 1972;250:20–6.
[6] Geil PH. Polymer reviews. Polymer single crystals, vol. 5. Baston, PA: Wiley; 1963.
[7] Hoffmann JD. Polymer 1979;20:1071–7.
[8] Smith P, Lemstra PJ. J Mater Sci 1980;15:505–14.
[9] Li CY, Li L, Cai W, Kodjie SL, Tenneti K. Adv Mater 2005;17:1198–202.
[10] Zhang XF, Liu T, Sreekumar TV, Kumar S, Hu XD, Smith K. Polymer 2004;45:8801–7.
[11] Ryan KP, Lipson SM, Drury A, Cadek M, Ruether M, O'Flaherly SM, et al. Chem Phys Lett 2004;391:329–33.
[12] Yudin VE, Svetlichnyi VM, Shumakov AN, Letenko DG, Feldman AY, Marom G. Macromol Rapid Commun 2005;26:885–8.
[13] Bhattacharyya AR, Sreekumar TV, Liu T, Kumar S, Ericson LM, Hauge RH, et al. Polymer 2003;44:2373–7.
[14] Mitchell CA, Krishnamoorti R. Polymer 2005;46:8796–804.
[15] Leelapornpisit W, Ton-That MT, Perrin-Sarazin F, Denault J. J Polym Sci Part B 2005;43:2445–53.
[16] Hsu WK, Li WZ, Zhu YQ, Grobert N, Terrones M, Terrones H, et al. Chem Phys Lett 2000;317:77–82.
[17] Minus M, Kumar S. Abstracts of papers, 229th ACS National Meeting, San Diego, CA, United States, March 13–17. Polym Mater: Sci Eng 2005; 92:149–50.
[18] Zhou W, Fischer JE, Heiney PA, Fan H, Davis VA, Pasquali M, et al. Phys Rev B 2005;72:0454402–0454405.
[19] Ryan KP, Cadek M, Drury A, Ruether M, Blau WJ, Coleman JN. Fullerenes Nanotubes Carbon Nanostruct 2005;13:431–4.
[20] Liu LQ, Barber AH, Nuriel S, Wagner HD. Adv Funct Mater 2005;15: 975–80.
[21] Rozhin AG, Sakakibara Y, Kataura H, Matsuzaki S, Ishida K, Achiba Y, et al. Chem Phys Lett 2005;405:288–93.
[22] Paiva MC, Zhou B, Fernando KAS, Lin Y, Kennedy JM, Sun YP. Carbon 2004;42:2849–54.
[23] Zhang XF, Liu T, Sreekumar TV, Kumar S, Moore VC, Hauge RH, et al. Nano Lett 2003;3:1285–8.
[24] Vigolo B, Penicaud A, Coulon C, Sauder C, Pailler R, Journet C, et al. Science 2000;290:1331–4.
[25] Dalton AB, Collins S, Munoz E, Razal JM, Ebron VH, Ferraris JP, et al. Nature 2003;423:703.
[26] Cha WI, Hyon SH, Ikada Y. J Polym Sci 1994;32:297–304.
[27] Assender HE, Windle AH. Polymer 1998;39:4295–302.
[28] Cullity BD. Elements of X-ray diffraction. Massachusetts: Addison-Wesley Publishing Company, Inc.; 1978 p. 102.
[29] Wilchinsky ZW. J Appl Phys 1960;31:1969–72.
[30] Bunn CW. Nature 1948;161:929.
[31] Klug HP, Alexander LE. X-ray diffraction procedures. USA: Wiley; 1954.
[32] Liu T, Kumar S. Chem Phys Lett 2003;378:257–62.
[33] Chae HG, Minus M, Kumar S. Polymer 2006;47:3494–3504.
[34] Wang ZL, Kang ZC. Functional and smart materials: structural evolution and stucture anaylsis. New York: Plenum Press; 1998 p. 350–1.
[35] Valentini L, Biagiotti J, Lopez-Manchado MA, Satucci S, Kenny JM. Polym Eng Sci 2004;44:303–11.
[36] García-Gutiérrez MC, Nogales A, Rued DR, Domingo C, García-Ramos JV, Broza G, et al. Polymer 2006;47:341–5.